Research Article | Vol. 13, No. 1 / 1 Jan 2022 / Biomedical Optics Express 222
Biomedical Optics EXPRESS

Molecular pathological recognition of freshly excised human glioma using terahertz ATR spectroscopy

NING MU,[1,4] CHUANYAN YANG,[1,4] DEGANG XU,[2,3] SHI WANG,[1] KANG MA,[1] YING LAI,[1] PEIWEN GUO,[1] SHUIXIAN ZHANG,[1] YUYE WANG,[2,3,5] HUA FENG,[1,6] TUNAN CHEN,[1,7] AND JIANQUAN YAO[2,3]

[1]*Department of Neurosurgery and Key Laboratory of Neurotrauma, Southwest Hospital, Third Military Medical University (Army Medical University), Chongqing 400038, China*
[2]*Institute of Laser and Optoelectronics, School of Precision Instruments and Optoelectronics Engineering, Tianjin University, Tianjin 300072, China*
[3]*Key Laboratory of Optoelectronics Information Technology (Ministry of Education), Tianjin University, Tianjin 300072, China*
[4]*Contributed equally*
[5]*yuyewang@tju.edu.cn*
[6]*fenghua8888@vip.163.com*
[7]*ctn@tmmu.edu.cn*

Abstract: The diagnosis and treatment of glioma depends greatly on the rapid extraction of molecular pathological features. In this study, human brain tumor tissues of different grades were analyzed using terahertz (THz) attenuated total reflectance (ATR) time-domain spectroscopy. Substantial differences in THz parameters were observed between paracarcinoma tissue and grade I-IV gliomas, Furthermore, the difference of THz absorption coefficient increases with the increase of THz frequency. It was also demonstrated that the isocitrate dehydrogenase (IDH) mutant and wild-type glioma tissues can be well distinguished using THz spectroscopy. Therefore, THz ATR spectroscopy can realize molecular typing recognition based on molecular pathology. This will provide a theoretical basis for developing intraoperative real-time glioma recognition and diagnosis technology.

1. Introduction

Gliomas are intracranial tumors that mostly occur in the functional regions of the brain and cause higher morbidity and mortality than other central nervous system (CNS) tumor types [1,2]. Despite many advances in the diagnosis and treatment of glioma, the therapeutic effects and prognosis have not improved substantially [3,4]. In the past, the pathological diagnosis of glioma was completely dependent on histology [5]. However, the current clinical practice advocates the integration of genetic information and traditional histology, to make new classification and comprehensive judgment [6,7]. The 2016 World Health Organization (WHO) classification of CNS tumors introduced the concept of molecular typing. Gliomas are divided into many subtypes [8,9], such as IDH mutant and wild-type diffuse gliomas, emphasizing the importance of the molecular characteristics of gliomas. The new classification utilizes a combination of genotype and phenotype, which can help clinicians understand the characteristics and development of glioma more accurately. It is used to not only grasp the homogeneity of clinical outcomes of patients with different molecular characteristics, but also clearly understand the heterogeneity that can occur within the same glioma diagnosis [6,10].

The rapid extraction of molecular pathological features of tumors is an important prerequisite for accurate diagnosis and clinical research of glioma [9,11]. The intraoperative and early

#445111 https://doi.org/10.1364/BOE.445111
Journal © 2022 Received 4 Oct 2021; revised 13 Nov 2021; accepted 13 Nov 2021; published 7 Dec 2021

Biomedical Optics EXPRESS

postoperative *in situ* diagnosis and treatment technology has also become an important area to improve the clinical treatment's effect. At present, the internationally developed program is "intraoperative magnetic resonance imaging (MRI) + neuronavigation + intraoperative pathological biopsy" [12–14]. However, this scheme has the disadvantages of expensive equipment and site construction, heavy economic burden on patients, increased operative time (by approximately 1 hour for intraoperative MRI and intraoperative pathology) and operating risks. Additionally, there are some logistical limitations, for example, MRI, rapid intraoperative pathological detection, and image navigation are disconnected in space and time, and it is difficult to achieve correspondence and mutual interpretation between microscopic pathology and macroscopic images [13,14].

Owing to the aggressiveness of glioma, the movement of intraoperative tissue can be difficult to follow accurately [10]. Moreover, due to the heterogeneity of gliomas, clinicians need to consider as many locations as possible in the intraoperative pathological examination to provide a better basis for decision making [15]. However, considering too many sites in an intraoperative pathological examination can be time consuming and result in an excessive workload for the pathologist, making it difficult to select an arbitrary number of pathological examination sites. Nonetheless, if the tumor molecular typing information can be obtained immediately and quickly during the operation, it can assist in the formulation of surgical strategies and provide earlier and more comprehensive molecular pathological information as a basis for the accurate delineation of tumor boundaries and the formulation of comprehensive postoperative treatment plans. Therefore, it would be very useful to identify new real-time, sensitive, and accurate glioma detection methods to assist tumor diagnosis.

To that end, terahertz (THz) technologies have emerged in recent years. THz radiation, in the frequency range of 0.1–10 THz, is between the far-infrared and microwave regions on the electromagnetic spectrum. The THz spectral region has some unique and useful characteristics, such as spectral fingerprints, safety, label-free detection, and water sensitivity in biological macromolecules, cells, and tissues. Therefore, the THz spectrum is particularly suitable for the *in vivo* detection of biological tissues [16], and THz spectral identification of various tumor tissues has become an area that has garnerd increased research interest in recent years [17–20]. Studies have shown that nuclear atypia and mitotic activity in glioma tissues are increased relative to those in normal brain tissues. To maintain the vitality of these cells, the vascular density and water content in the glioma region are increased, Thereby, affecting the refractive index and absorption coefficient [21]. A newly isolated glioma [22,23] and paraffin-embedded glioma [23] have been previously used in THz spectroscopy studies, which proved that THz radiation could be used for identifying glioma regions. The above evidence indicates that the terahertz spectrum technology is promising for achieving in situ pathological identification. However, the previous studies mainly focused on the following aspects: (1) discrimination between normal and abnormal tissues and identification of malignant tissue [21,23]; and (2) bridging the gap from *in vitro* sample detection to *in vivo* detection [23–26]. There are no studies on THz physical characterization based on molecular typing, and there are few studies on human glioma tissues, none of which could completely simulate the tumor microenvironment of patients.

THz time-domain spectroscopy is one of the effective coherent detection techniques that can obtain phase and intensity information at the same time. Generally, the transmission and reflection modes are widely used in THz time-domain spectroscopy system. However, the thickness of sample with high water content needs to be strictly controlled in transmission mode since water has strong absorption effect on THz wave. For reflection mode, the complex reference calibrations are necessary to reduce the effect of diffuse reflection and interference [27]. Attenuated total reflection (ATR) mode can provide information on the interaction between the sample and evanescent wave traveling along a prism surface, which can ensure the sample integrity and has the characteristic of high sensitivity [28]. Therefore, THz-ATR mode is an

Biomedical Optics EXPRESS

ideal tool for analyzing the THz spectral properties of biological samples without pre-processing or labeling.

In this study, human brain tumor tissues of different grades were analyzed using THz attenuated total reflectance (ATR) time-domain spectroscopy. The spectral characteristics of glioma tissues of different grades and paracarcinoma tissues differed in the range of 0.5–2.0 THz. Furthermore, the IDH mutant and wild types can be well distinguished with THz spectra. These results demonstrate that THz ATR spectroscopy can be used for glioma molecular typing recognition. This will help the realization of real-time pathological identification, diagnosis, and treatment during surgery, and the provision of a more precise treatment plan for patients.

2. Methodology

2.1. Experiment setup

The THz time-domain spectroscopy system (Japan, Advantest, TAS7500SP) with attenuated total reflection (ATR) mode was used in the experiment. The spectral range was in the range of 0.2–2.5 THz with the scanning frequency resolution of 7.6 GHz. Figure 1 shows the schematic diagram of the experiment setup. The THz wave was radiated using a GaAs-photoconductive emitter. After passing through the off-axis parabolic mirror, the terahertz wave was focused on the upper surface of the ATR prism. A Dove prism made of Si crystal ($n = 3.42$ in THz range), was fixed at the focal position of the incident THz wave (p polarized) [29]. Through comprehensive consideration of the sample size [30], the attenuation rate [29,31]and the penetration depth [31] of THz wave, the incident angle of THz wave was chosen to be 57° in this experiment. In this case, the THz focal beam size was 2 mm at 1 THz. When the incident angle was larger than the critical angle, the attenuated total internal reflection occurred on the upper surface of the ATR prism, and the evanescent wave interacted with the tissues to be tested. Subsequently, the terahertz wave carrying the sample information, was collected using the photoconductive detector and transmitted to the computer data analysis module. Considering the penetration depth of the evanescent wave in distilled water at 1 THz is 24 μm, the sample thickness used for each measurement was chosen to be greater than 0.5 mm. Multiple tests of different samples were carried out to make sure that the signals from repeated measurements can be overlapped in a certain time. Finally, the terahertz spectral information of the tumor was obtained and analyzed. All the measurements were performed at a temperature of 25°C and at a relative humidity (RH) of 1%.

2.2. Summary of patient pathological information

All specimens were collected from the Southwest Hospital, Third Military Medical University, China. All experiments were approved by the ethics committee of the Southwest Hospital of Third Military Medical University (Army Medical University) (No. (B)KY2021043). Herein, we detected fresh human glioma of different WHO grades and its peritumoral tissues in vitro using THz ATR technology, and obtained the physical parameters in the range of 0.5–2 THz. Summary information of the 12 samples of human brain gliomas *ex vivo* is listed in Table 1, as provided by the Department of Neurosurgery, Southwest Hospital. Samples were obtained from 7 males and 5 females, aged 20–64 years old, with an average age of 46.25 ± 14.02 years. All patients were diagnosed with glioma via magnetic resonance imaging (MRI), histopathology and cytology (the specific pathological classification is as given in the Table 1). According to the 2016 WHO classification standard, there were no cases of grade I, four cases of grade II, four cases of grade III, and four cases of grade IV. In some cases, we also preserved the paracarcinoma tissue (adjacent to the glioma). Figure 2 shows the MRI images of case 7, diagnosed as a typical left frontal lobe glioma patient. Figures 2(a) and 2(b) are the results of T1 and T2 signals, respectively, which show high-intensity signals with unrestricted dispersion. Figure 2(c) shows

Biomedical Optics EXPRESS

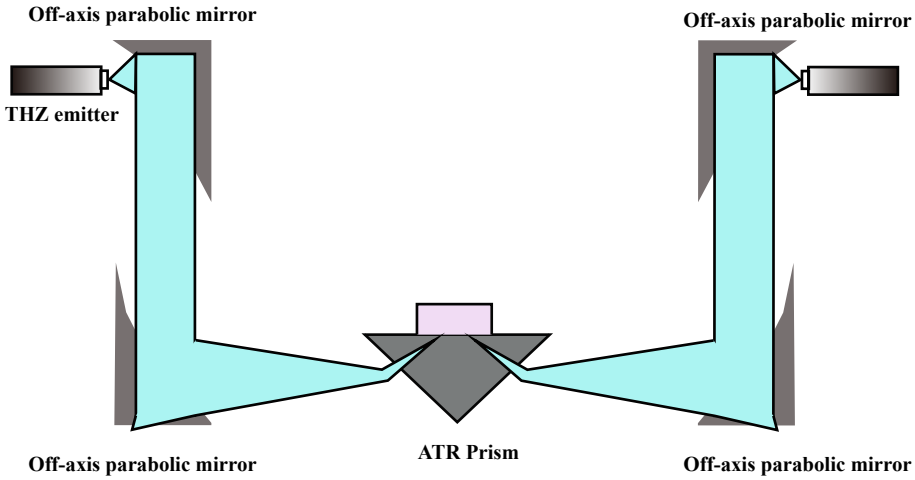

Fig. 1. Experimental setup of the terahertz time-domain attenuated total reflectance spectroscopy system.

the image of dynamic contrast-enhanced MRI. The enhanced high-density round sector is the tumor body, the edema region is the area around the glioma with a low-density signal. The size of the tumor is 3.3×2.4×3.1cm^3, according to the image. The glioma caused a slight midline structure shifting to the right and subtentorial cerebellar and brain stem abnormalities. The DTI result in Fig. 2(d) illustrates that the tumor destroyed association fibers in the left cerebral hemisphere.

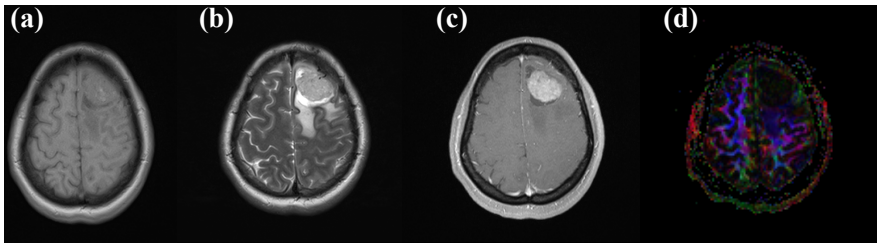

Fig. 2. Magnetic resonance images of a patient (No. 7): (a) T1W1, (b) T2W1, (c) PW1/DSC (d) DTI.

2.3. Sample measurement

A standardized experimental scheme has been established for sample preparation and THz measurement. Before performing the spectroscopic analysis of human tumor samples, measurement of the air medium was performed as the reference. Considering that the tissues were cryopreserved and cell lysis might have occurred, and a large amount of biological tissue fluid might have spread outside the human tissue. To eliminate the effects of tissue fluid on terahertz spectroscopy, the samples were thawed, and all the residual tissue fluid on the surface was gently

Biomedical Optics EXPRESS

Table 1. Summary of the pathological information of the patients[a]

Case	Age	Sex	Pathology	WHO grade	IDH 1	Ki-67 (%)	MGMT	1p/19q	Para-
1	49	F	Anaplastic astrocytoma	III	Mutant	8	-		
2	61	F	Glioblastoma	IV	WT	20	-		+
3	43	M	Astrocytoma	II	Mutant	5	-		
4	51	M	Anaplastic Oligodendroglioma	III	Mutant	7	-	+	
5	26	M	Diffuse astrocytoma	II	Mutant	5	-		
6	52	F	Anaplastic astrocytoma	III	WT	8	-		
7	42	F	Oligodendroglioma	II	WT	10	-	+	
8	20	M	Pilomyxiod astrocytoma	II	WT	3	-		
9	61	M	Glioblastoma	IV	WT	30	-		
10	33	F	Glioma	IV	WT	-	-		+
11	53	M	Anaplastic astrocytoma	III	Mutant	7	-		+
12	64	M	Gliosarcoma	IV	WT	30	-		

[a]WHO grade: World health Organization; Ki-67(%): *Ki*-67 positive rate; para-: para-carcinoma tissue; 1p/19q: 1p/19q absence.

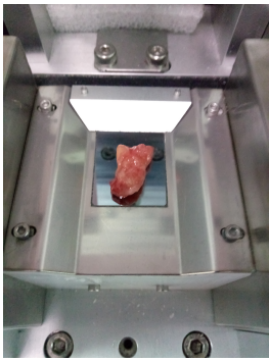

Fig. 3. The illustration of human glioma measurement by THz-ATR.

removed using lens paper. Thereafter, the samples were placed on the surface of the ATR prism and pressed gently to ensure that they adhered tightly to the upper surface of the ATR prism and covered all the terahertz spots, as shown in Fig. 3. To ensure the accuracy of the experimental results, the operation time of temperature (25°C), surface humidity (1% RH), and suction tissue fluid were strictly controlled during the operation time. Each sample was tested five times to verify the repeatability.

3. Principles

The attenuated total internal reflection occurred on the surface on the ATR prism, and the relationship between the output signal and input signal was determined from the reflectivity and

Biomedical Optics EXPRESS

phase shift. The THz time-domain waveforms of the reference and sample measurements are Fourier transformed to acquire the frequency-dependent parameters $E_{ref}(\omega)$ and $E_{sam}(\omega)$. Thus, the reflectivity $R(\omega)$ and the phase shift $\varphi(\omega)$ can be expressed as follows:

$$R(\omega) = \left|\frac{E_{sam}(\omega)}{E_{ref}(\omega)}\right|^2 = \left|\frac{r_{sam}(\omega)}{r_{ref}(\omega)}\right|^2 \tag{1}$$

$$\Delta\varphi(\omega) = Arg\left(\frac{r_{sam}(\omega)}{r_{ref}(\omega)}\right) \tag{2}$$

Here, $r_{sam}(\omega)$ denotes the reflection coefficient of the prism–sample interface, and $r_{ref}(\omega)$ represents the reflection coefficient of the prism–air interface. For p-polarized THz wave, $r_{sam}(\omega)$ and $r_{ref}(\omega)$ satisfy the following equations, respectively.

$$r_{sam}(\omega) = \frac{\tilde{n}_2^2(\omega)\cos\theta - i\tilde{n}_1(\omega)\sqrt{\tilde{n}_1^2(\omega)\sin^2\theta - \tilde{n}_2^2(\omega)}}{\tilde{n}_2^2(\omega)\cos\theta + i\tilde{n}_1(\omega)\sqrt{\tilde{n}_1^2(\omega)\sin^2\theta - \tilde{n}_2^2(\omega)}} \tag{3}$$

$$r_{ref}(\omega) = \frac{\tilde{n}_3^2(\omega)\cos\theta - i\tilde{n}_2(\omega)\sqrt{\tilde{n}_2^2(\omega)\sin^2\theta - \tilde{n}_3^2(\omega)}}{\tilde{n}_3^2(\omega)\cos\theta + i\tilde{n}_2(\omega)\sqrt{\tilde{n}_2^2(\omega)\sin^2\theta - \tilde{n}_3^2(\omega)}} \tag{4}$$

Here, θ denotes the incident angle of THz wave at the prism detection surface, and it is 57° in the experiment. $n_1(\omega)$, $n_2(\omega)$ and $n_3(\omega)$ represent the refractive indices of the ATR prism, sample and air, respectively. By combining Eq. (3) and Eq. (4), we can obtain the reflection coefficient of THz wave at the sample-prism interface,

$$r_{sam}(\omega) = r(\omega)\exp[\Delta\varphi(\omega) - 3.02] \tag{5}$$

The complex permittivity of the sample can be expressed as follows:

$$\tilde{\varepsilon}_{sam}(\omega) = \tilde{n}_{sam}^2(\omega) = \frac{A(\omega) \pm \sqrt{A^2(\omega) - B(\omega)\sin^2 2\theta}}{2B(\omega)\cos^2\theta} \times \tilde{n}_{prism}^2(\omega) \tag{6}$$

Where $A(\omega)=(r_{sam}(\omega)+1)^2$and $B(\omega)=(r_{sam}(\omega)-1)^2$. We chose the solution with a positive imaginary part as the complex dielectric constant and complex refractive index. According to $\tilde{n}_{sam}(\omega)=n_{sam}(\omega)+j\kappa_{sam}$ and Eq.6, the refractive index n_{sam} and extinction coefficient κ_{sam} of sample can be calculated as follows:

$$n_{sam} = \sqrt{\frac{\sqrt{(\mathrm{Re}(\varepsilon_{sam}))^2 + (\mathrm{Im}(\varepsilon_{sam}))^2} + \mathrm{Re}(\varepsilon_{sam})}{2}} \tag{7}$$

$$\kappa_{sam} = \sqrt{\frac{\sqrt{(\mathrm{Re}(\varepsilon_{sam}))^2 + (\mathrm{Im}(\varepsilon_{sam}))^2} - \mathrm{Re}(\varepsilon_{sam})}{2}} \tag{8}$$

Furthermore, the absorption coefficient $\alpha_{sam}(\omega)$ of the sample can be expressed as follows,

$$\alpha_{sam}(\omega) = \frac{2\omega\kappa}{c} = \sqrt{\frac{\sqrt{(\mathrm{Re}(\varepsilon_{sam}))^2 + (\mathrm{Im}(\varepsilon_{sam}))^2} - \mathrm{Re}(\varepsilon_{sam})}{c}} \times \sqrt{2}\omega \tag{9}$$

Here, c is the speed of THz wave in vacuum.

Biomedical Optics EXPRESS

4. Results and discussion

The samples of 12 patients with glioma were included in this study, of which three cases contained paracarcinoma tissue adjacent to the tumor (as shown in Table 1). To verify the identification of the glioma boundary using terahertz technology, we used THz spectroscopy to analyze 12 glioma samples and 3 paracarcinoma tissue samples as listed in Table 1. The THz spectra were calculated by averaging over the obtained data, as shown in Fig. 4. The standard deviation was shown as error bars. As shown in Fig. 4(a), the absorption coefficient of both the paracarcinoma and glioma tissues increased with the increase of THz frequency. The absorption coefficient of glioma was significantly higher than that of paracarcinoma tissue within the 0.5–2.0 THz range. The difference in absorption coefficient between the two kinds of tissues became more pronounced with the increase of THz frequency as well despite the large error value above 1.5 THz. Consistently, Fig. 4(b) showed the extinction coefficient of the gliomas was substantially higher than that of the paracarcinoma tissues. The refractive index of glioma tissue was lower than that of paracarcinoma tissues, and the difference also increased at higher frequencies, as shown in Fig. 4(c). Overall, it is reasonable to deduce that higher THz frequency was preferred for the THz identification of brain glioma with better contrast on the condition of enough THz power. Therefore, glioma tissue and paracarcinoma tissues can be clearly distinguished in the range of 0.5–2.0 THz, thereby demonstrating the utility of this technique for tissue analysis.

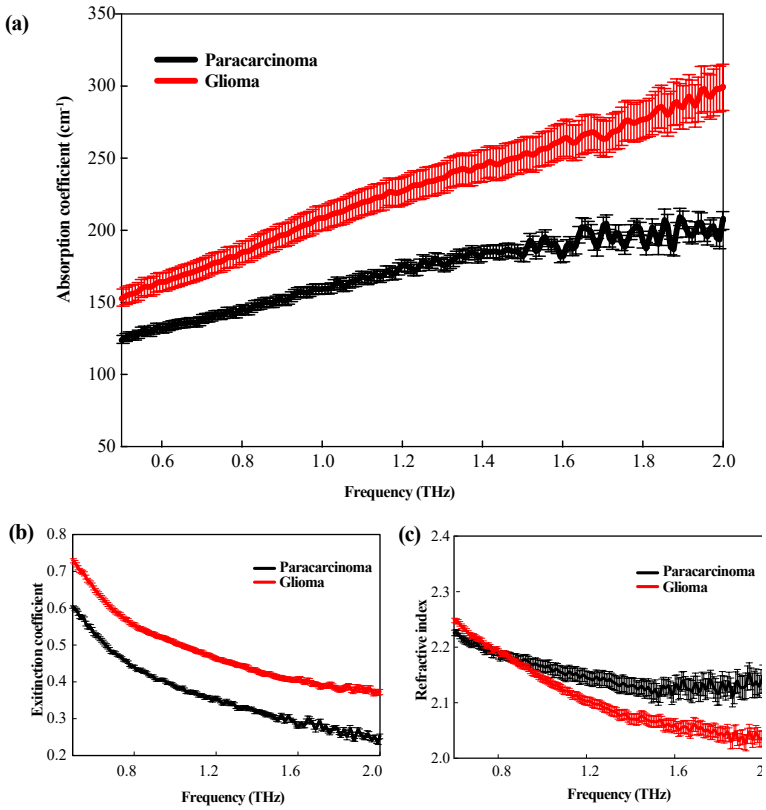

Fig. 4. THz spectral curves of paracarcinoma and glioma tissues (a) absorption coefficient, (b) extinction coefficient, and (c) refractive index.

Another tool that clinician often use during surgery to determine the tumor boundary is rapid hematoxylin–eosin staining. Figure 5 showed the staining of different sections from

Biomedical Optics EXPRESS

the paracarcinoma tissue to the tumor tissue. Figure 5(a–d) show the progression from the paracarcinoma tissue to the tumor tissue, the nuclei become more hyperchromatic and the nuclear atypia becomes more severe, and cell distribution gradually becomes scattered, with the glioma nuclei being deeply stained and wrinkled and the tissue showing serious edema. These results are consistent with the tumor morphological features. More specifically, compared with the cells in paracarcinoma tissue, glioma cells are round to oval in shape and rich in lightly stained cytoplasm; Conversely, their nuclei are large and deeply stained, showing evidence of mitosis, and the tumor cells are distributed in a diffuse, flaky arrangement [32,33]. The water content of tumor tissue is higher than that of normal tissue and THz spectroscopy is extremely sensitive to water. This result is consistent with that reported by Wahaia [34,35].

THz spectra can be affected by some factors other than water. Usually, immunohistochemical tests are used for molecular pathological diagnosis of tumor tissues removed during surgery. Figure 6 shows the immunohistochemical results of CD34, a diagnostic marker of tumor angiogenesis. The positive expression of CD34 was localized in the cell membrane and cytoplasm of tumor vascular endothelial cells and paracarcinoma vascular endothelial cells. Compared with the paracarcinoma tissue, CD34 expression in the glioma was strongly positive, i.e., compared with paraneoplastic tissues, the vascular density in the tumor is increased as show in Fig. 6(a–d). Therefore, in addition to water content in tissue, factors such as vascular density and the vascular epidermis can also affect the THz spectral parameters.

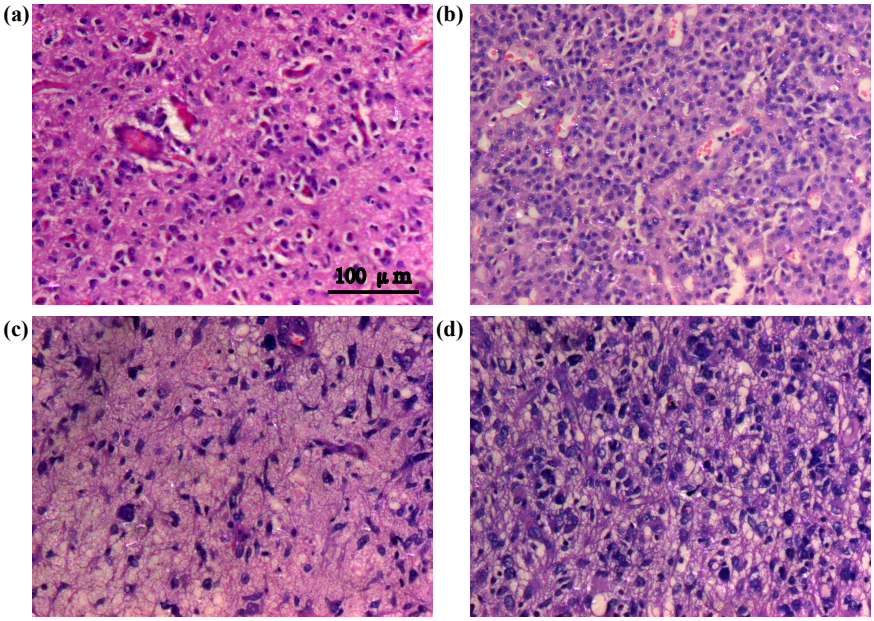

Fig. 5. Intraoperative hematoxylin–eosin staining (a–d) series from paracarcinoma tissue to glioma tissue.

Subsequently, the feasibility of terahertz technology to identify pathological grades of gliomas was evaluated. According to the clinicopathological diagnosis, glioma samples were divided into low-grade (grade I–II, four samples) and high-grade groups (grade III–IV, eight samples), as shown in Table 1. It is well known that the Ki-67 labeling index can be used to evaluate the mitotic activity of tumor cells, and Ki-67 expression can indicate the degree of tumor cell proliferation, the different states of the cell cycle and the value-added rate of tumor cells. In

Biomedical Optics EXPRESS

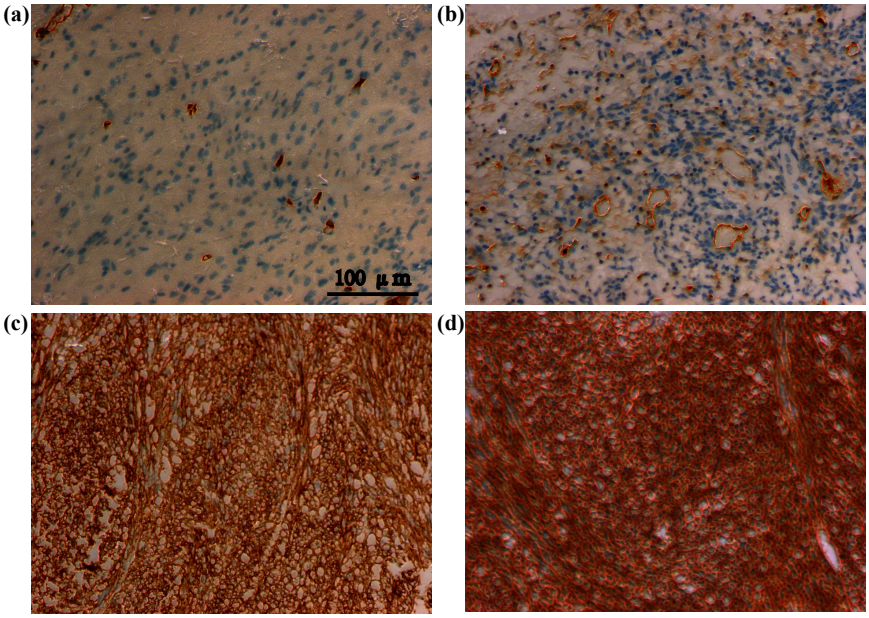

Fig. 6. CD34 (vascular marker) expression (a–d) series from paracarcinoma tissue to glioma tissue.

recent years, some researches have measured the expression of Ki-67 (determined according to the number of positive cells) to detect the percentage of value-added cells, in order to determine the value-added activity of tumor cells, and then predict the survival time in a given histological grade [36–38]. We performed immunohistochemical staining of Ki-67 in gliomas of different grades. As shown in Fig. 7, there are different degrees of positive expression of Ki-67 in the glioma samples, and the degree of positive expression increases with malignancy, which is consistent with the results of previous research [39].

Figure 8 depicts the terahertz spectroscopy of low-grade (I–II) and high-grade (III–IV) glioma tissues. As shown in Fig. 8(a), the absorption coefficients differ only slightly between high- and low-grade gliomas, although the difference increased at higher THz frequencies. Although the difference is not significant, terahertz metamaterials and other technologies can be used to enhance the electromagnetic response and improve the analytical sensitivity [40]. However, there were no substantial differences in extinction coefficient or refractive index between the high- and low-grade gliomas, as shown in Fig. 8(b) and (c). This result suggests that the absorption coefficient at higher THz frequencies would be preferred for the pathological grading. That is perhaps because traditional pathological classification is mainly refers to macroscopic morphological features in clinic, as shown in Fig. 5. These observations are dependent on the subjective judgment of the pathologist and may include characteristics such as nucleotropy, mitosis, microvascular hyperplasia, local necrosis, etc. Furthermore, the degree of Ki-67 expression only indicates the proliferation characteristics of cells, whereas the THz spectrum essentially represents the collective vibration and rotational mode differences of the biological molecules (mainly proteins) contained therein [41]. However, the difference in Ki-67 expression will also affect cell morphology and angiogenesis, thereby affecting the absorption coefficient in the THz spectrum.

Biomedical Optics EXPRESS

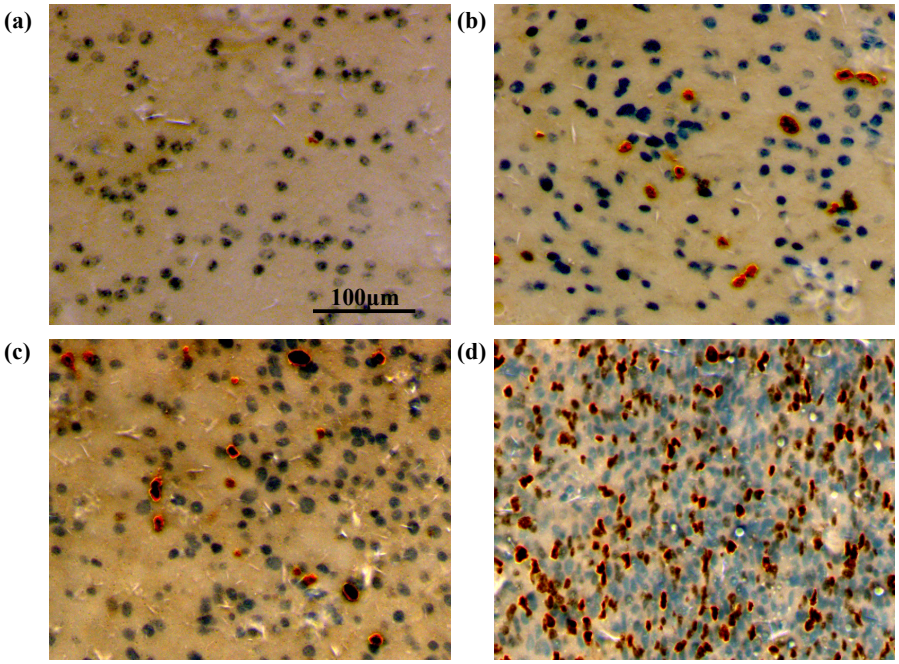

Fig. 7. Immunohistochemical analysis of Ki-67 showing different degrees of positive expression (a) 1%, (b) 6%, (c) 12%, and (d) 31%.

In recent years, a consensus has been reached that molecular typing is more likely to reveal the objective natural differences of tumors; that is, the population monoclonality of tumor cells will show specific protein molecular sets in specific tissue cells. Therefore, we attempted to use THz spectroscopy to detect different molecular types of glioma tissues. A common mutation in that occurring in gliomas is the isocitrate dehydrogenase (IDH) mutation. It has been found that 12% of glioblastoma patients had the IDH1 mutation [42,43]. Amidst the discovery of more and more new molecular markers, the IHD1 mutation has become one of the most stable and widely used molecular markers in glioma research. Some previous studies have also shown that glioma patients with the IDH1 mutation have a better prognosis than those with other gene mutations [44,45]. The progression-free survival periods and overall survival time of these patients are significantly longer than those of glioma patients with other gene mutations [46,47]. This suggests that there is a close relationship between the patients prognosis and the IDH1 gene mutation [48]. Therefore, the THz spectra of the IDH mutant and wild-types were further measured. Figure 9 shows an immunohistochemical image of a molecular marker for the IDH1 mutation. Figure 9(a) and 9(b) exhibit the IDH-1 wild-type and IDH-1 mutation positive, respectively. Wild-type IDH-1 refers to the normal expression of IDH protein in the tumor, while the mutant type refers to the base mutation resulting in the non-normal expression of IDH1. As Fig. 10(a) shows, the absorption coefficients of IDH1 mutant gliomas were higher than those of the IDH1 wild-type gliomas in the frequency range 0.5–2.0 THz. Figure 10(b) and 10(c) show that there is small differences in the refractive index and extinction coefficient between the IDH1 wild-type and the IDH1 mutant samples, although the error bars show some overlap. Thus, the absorption coefficient derived from THz spectrum recognition technology can realize molecular typing recognition based on molecular pathology. Current studies have confirmed

Biomedical Optics EXPRESS

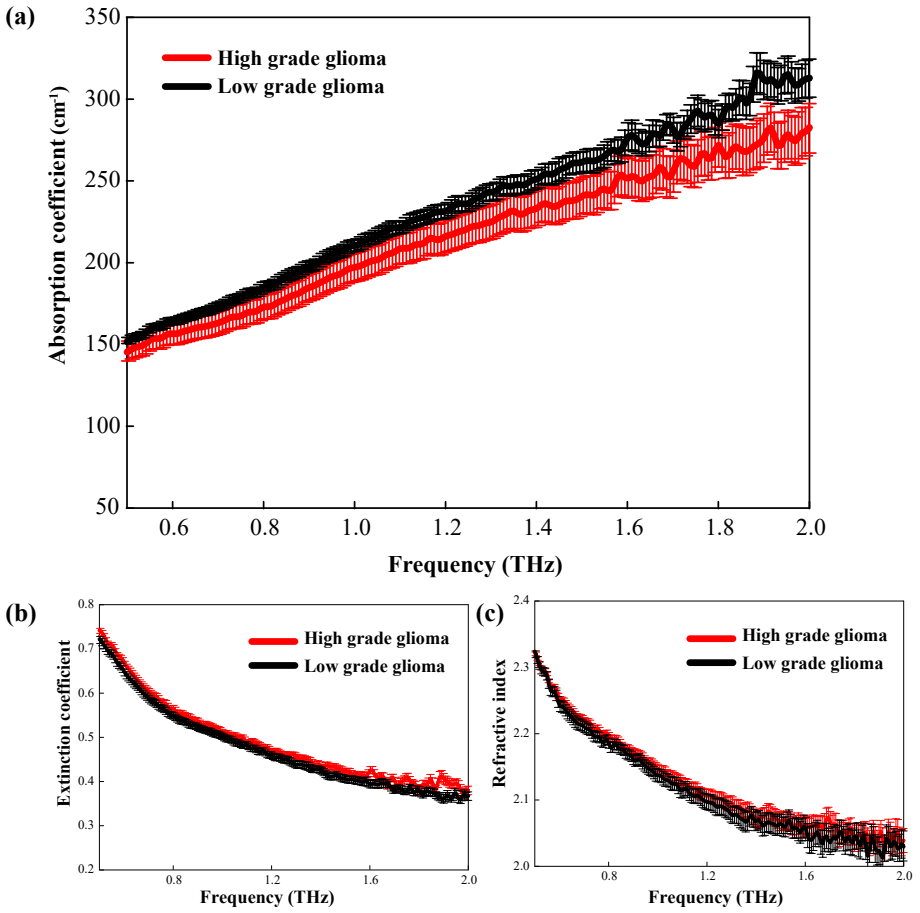

Fig. 8. THz spectrum curve for different degrees of glioma (a) absorption coefficient, (b) extinction coefficient, and (c) refractive index.

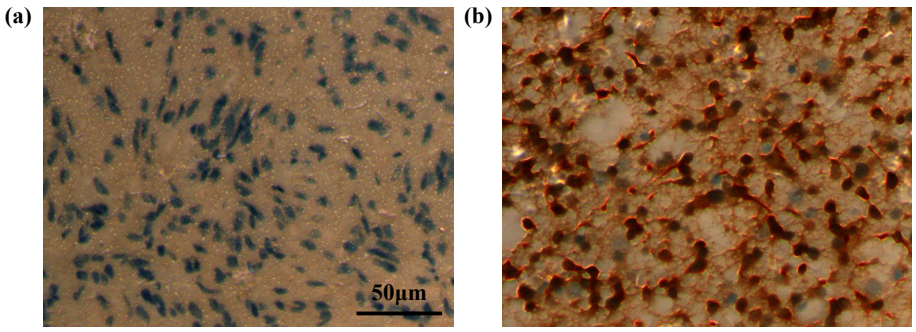

Fig. 9. Immunohistochemical analysis of IDH1(a) IDH-1 wild-type sample, (b) IDH-1 mutant positive sample.

Biomedical Optics EXPRESS

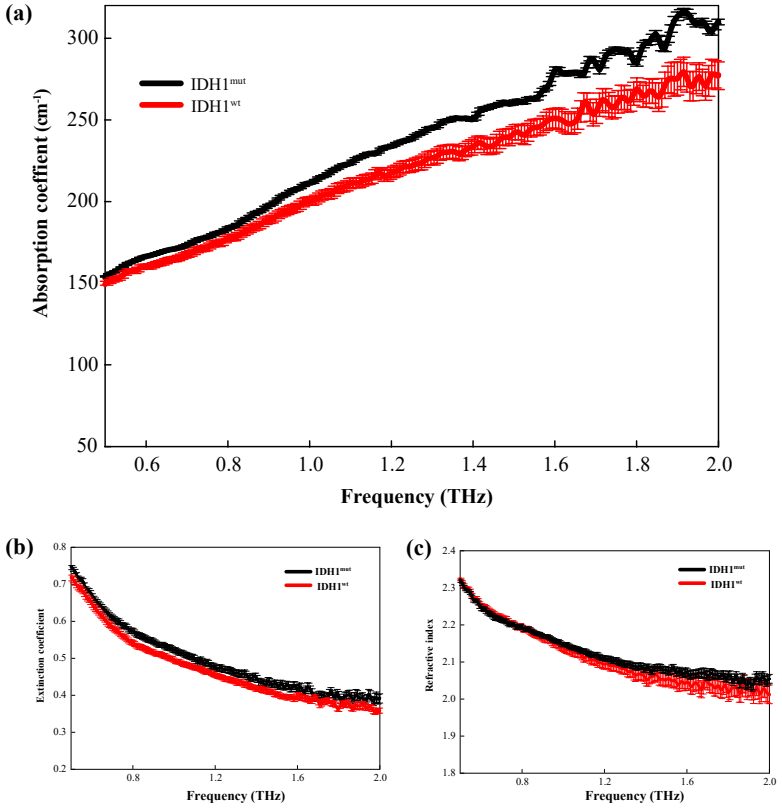

Fig. 10. THz spectrum curve for IDH^{wt} and IDH^{mut}: (a) absorption coefficient, (b) extinction coefficient, and (c) refractive index.

that excessive 2-HG metabolites will be produced in cells after IDH1 mutation, thus metabolic changes will induce epigenetic inheritance, such as genome and histone protein hypermethylation [42,49]. Chen et al. has identified 2-HG isomers using terahertz spectroscopy technology, and the molecular configuration has a good response and recognition characteristics to terahertz waves [50]. Meanwhile, Chen et al. also detected 5-methylcytosine, the methylation product of cytosine, using terahertz time-domain spectroscopy, they demonstrated the peak difference between cytosine and methylcytosine in terahertz time-domain spectra through theoretical and experimental perspectives [51]. Thus, the tumor tissue metabolites and gene methylation can be effectively identified by THz technology, which contribute to tumor molecular typing.

5. Conclusion

In conclusion, we studied the frequency-dependent THz properties of *ex vivo* human brain gliomas of different WHO grades to analyze the potential of THz technology for intraoperative neurodiagnosis. Our results show that THz spectroscopy can adequately distinguish the glioma tissue from the paracarcinoma tissue and that there are significant differences in the absorption coefficient, extinction coefficient, and refractive index between the glioma tissue and paracarcinoma tissue. It was found that the absorption coefficient at higher THz frequencies would be preferable for pathological grading. It was also found that IDH1 wild-type and IDH1 mutant gliomas could be well distinguished using the THz absorption coefficient. Therefore,

Biomedical Optics EXPRESS

THz ATR spectroscopy can be used for glioma molecular typing recognition. This technology is expected to achieve real-time pathological recognition.

Funding. National Natural Science Foundation of China (82173388); Army Medical University (2019MPRC021).

Disclosures. The authors declare that there are no conflicts of interest related to this article.

Data availability. Data underlying the results presented in this paper are not publicly available at this time but may be obtained from the authors upon request.

References

1. Q.T. Ostrom, L. Bauchet, F.G. Davis, I. Deltour, J.L. Fisher, C.E. Langer, M. Pekmezci, J.A. Schwartzbaum, M.C. Turner, K.M. Walsh, M.R. Wrensch, and J.S. Barnholtz-Sloan, "The epidemiology of glioma in adults: a "state of the science" review," Neuro-Oncology **16**(7), 896–913 (2014).
2. M. Weller, W. Wick, K. Aldape, M. Berger, S.M. Pfister, R. Nishikawa, M. Rosenthal, P.Y. Wen, R. Stupp, and G. Reifenberger, "Glioma," Nature Reviews Disease Primers **1**, 15017 (2015).
3. P.Y. Wen and S. Kesari, "Malignant gliomas in adults," N. Engl. J. Med. **359**(5), 492–507 (2008).
4. H. Ohgaki and P. Kleihues, "Population-based studies on incidence, survival rates, and genetic alterations in astrocytic and oligodendroglial gliomas," J Neuropathol Exp Neurol **64**(6), 479–489 (2005).
5. D.N. Louis, H. Ohgaki, O.D. Wiestler, W.K. Cavenee, P.C. Burger, A. Jouvet, B.W. Scheithauer, and E. Kleihues, "The 2007 WHO classification of tumours of the central nervous system," Acta Neuropathol. **114**(2), 97–109 (2007).
6. D.N. Louis, "The next step in brain tumor classification: "Let us now praise famous men"... or molecules?" Acta Neuropathol **124**(6), 761–762 (2012).
7. G. Reifenberger, H.G. Wirsching, C.B. Knobbe-Thomsen, and M. Weller, "Advances in the molecular genetics of gliomas-implications for classification and therapy," Nat Rev Clin Oncol **14**(7), 434–452 (2017).
8. J. Buckner, C. Giannini, J. Eckel-Passow, D. Lachance, I. Parney, N. Laack, and R. Jenkins, "Management of diffuse low-grade gliomas in adults-use of molecular diagnostics," Nat Rev Neurol **13**(6), 340–351 (2017).
9. J. Hainfellner, D.N. Louis, A. Perry, and P. Wesseling, "International Society of Neuropathology-Haarlem Consensus Guidelines for Nervous System Tumor Classification and Grading," Brain Pathology **24**(6), 671–672 (2014).
10. Cancer Genome Atlas Research Network, "Comprehensive, integrative genomic analysis of diffuse lower-grade gliomas," N Engl J Med **372**(26), 2481–2498 (2015).
11. D.N. Louis, A. Perry, P. Wesseling, D.J. Brat, I.A. Cree, D. Figarella-Branger, C. Hawkins, H. K. Ng, S. M. Pfister, G. Reifenberger, R. Soffietti, D.A. Von, and D.W. Ellison, "The 2021 WHO Classification of Tumors of the Central Nervous System: a summary," Neuro-Oncology (2021)
12. T.J. Brown, M.C. Brennan, M. Li, E.W. Church, N.J. Brandmeir, K.L. Rakszawski, A.S. Patel, E.B. RIzk, D. Suki, R. Sawaya, and M. Glantz, "Association of the extent of resection with survival in glioblastoma: a systematic review and meta-analysis," JAMA Oncol **2**(11), 1460 (2016).
13. M. Jansen, S. Yip, and D.N. Louis, "Molecular pathology in adult gliomas: diagnostic, prognostic, and predictive markers," The Lancet Neurology **9**(7), 717 (2010).
14. K.R. Swanson, G. Chakraborty, C.H. Wang, R. Rockne, H.L. Harpold, M. Muzi, T.C. Adamesen, K.A. Krohn, and A.M. Spence, "Complementary but distinct roles for MRI and 18F-fluoromisonidazole PET in the assessment of human glioblastomas," J Nucl Med **50**(1), 36–44 (2009).
15. J.G. Nicholson and H.A. Fine, "Diffuse glioma heterogeneity and its therapeutic implications," Cancer Discov **11**(3), 575–590 (2021).
16. J. Xu, K.W. Plaxco, and S.J. Allen, "Probing the collective vibrational dynamics of a protein in liquid water by terahertz absorption spectroscopy," Protein Sci. **15**(5), 1175–1181 (2006).
17. C Hua, T.H. Chen, T.F. Tseng, J.T. Lu, and C.K. Sun, "High-sensitivity in vivo THz transmission imaging of early human breast cancer in a subcutaneous xenograft mouse model," Opt. Express **19**(22), 21552 (2011).
18. Y.C. Sim, J.Y. Park, K. Ahn, C. Park, and J. Son, "Terahertz imaging of excised oral cancer at frozen temperature," Biomed. Opt. Express **4**(8), 1413 (2013).
19. R.M. Woodward, V.P. Wallace, R.J. Pye, B.E. Cole, and M. Pepper, "Terahertz pulse imaging of ex vivo basal cell carcinoma," J Invest Dermatol. **120**(1), 72–78 (2003).
20. C.B. Reid, A. Fitzgerald, G. Reese, R. Goldin, P. Tekkis, P.S. O'Kelly, A.P. Gibson, and V.P. Wallace, "Terahertz pulsed imaging of freshly excised human colonic tissues," Phys. Med. Biol. **56**(14), 4333 (2011).
21. S. Yamaguchi, Y. Fukushi, O. Kubota, T. Itsuji, T. Ouchi, and S. Yamamoto, "Origin and quantification of differences between normal and tumor tissues observed by terahertz spectroscopy," Phys. Med. Biol. **61**(18), 6808 (2016).
22. S.J. Oh, Y. Huh, S.H. Kim, J. Yang, K. Jeong, Y. Park, J.H. Son, and J.S. Suh, "Terahertz pulse imaging of fresh brain tumor," *2011 International Conference on Infrared. Millimeter, and Terahertz Waves 2011 International Conference on Infrared, Millimeter, and Terahertz Waves*, 1–2 (2011).
23. K. Meng, T.N. Chen, C. Tao, L.G. Zhu, Q. Liu, F. Li, S.C. Zhong, Z.R. Li, and H. Feng, "Terahertz pulsed spectroscopy of paraffin-embedded brain glioma," J. Biomed. Opt **19**(7), 077001 (2014).
24. Y.Y. Wang, Z.N. Jiang, D.G. Xu, T.N. Chen, B.K. Chen, S. Wang, N. Mu, H. Feng, and J.Q. Yao, "Study of the dielectric characteristics of living glial-like cells using terahertz ATR spectroscopy," Biomed. Opt. Express **10**(10), 5351–5361 (2019).

Biomedical Optics EXPRESS

25. L.M. Wu, D.G. Xu, Y.Y. Wang, B. Liao, Z.N. Jiang, L. Zhao, Z.C. Sun, N. Wu, T.N. Chen, H. Feng, and J.Q. Yao, "Study of in vivo brain gliomas in mouse model using continuous-wave terahertz reflection imaging," Biomed. Opt. Express **10**(8), 3953–3962 (2019).
26. P.C. Ashworth, E. Pickwell-Macpherson, E. Provenzano, S.E. Pinder, and V.P. Wallace, "Terahertz pulsed spectroscopy of freshly excised human breast cancer," Opt. Express **17**(15), 12444–54 (2009).
27. Y.F. Wang, Y.Y. Wang, D.G. Xu, L.M. Wu, G.Q. Wang, B.Z. Jiang, T.Y. Yu, C. Chang, T.N. CHen, and J.Q. Yao, "Interference elimination based on the inversion method for continuous-wave terahertz reflection imaging," Optics Express **28**(15), 21926–21939 (2020).
28. H. Hirori, K. Yamashita, M. Nagai, and K. Tanaka, "Attenuated total reflection spectroscopy in time domain using terahertz coherent pulses," Jpn. J. Appl. Phys **43**(No. 10A), L1287–L1289 (2004).
29. H.X. Liu, Y.Y. Wang, D.G. Xu, Z.N. Jiang, J.N. Li, C. Yan, L.T. Tang, Y.X. He, D.X. Yan, X. Ding, H. Feng, and J.Q. Yao, "Optimization for vertically scanning terahertz attenuated total reflection imaging," Optics Express **26**(16), 20744–20757 (2018).
30. L.M. Wu, D.G. Xu, Y.Y. Wang, Y.Y. Zhang, H.J. Wang, B. Liao, S. Gong, T.N. Chen, N. Wu, H. Feng, and J.Q. Yao, "Horizontal-scanning attenuated total reflection terahertz imaging for biological tissues," Neurophoton. **7**(2), 025005 (2020).
31. H.X. Liu, Y.Y. Wang, D.G. Xu, L.M. Wu, C. Yan, D.X. Yan, L.H. Tang, Y.X. He, H. Feng, and J.Q. Yao, "High-sensitivity attenuated total internal reflection continuous-wave terahertz imaging," J. Phys. D: Appl. Phys. **50**(37), 375103 (2017).
32. O.A. Smolyanskaya, N.V. Chernomyrdin, A.A. Konovko, K.I. Zaytsev, I.A. Ozheredov, O.P. Cherkasova, M.M. Nazarov, J.P. Guillet, S.A. Kozlov, and Y.V. Kistenev, "Terahertz biophotonics as a tool for studies of dielectric and spectral properties of biological tissues and liquids," Prog. Quantum Electron. **62**, 1–77 (2018).
33. T.Y. Reynolds, S. Rockwell, and P.M. Glazer, "Genetic instability induced by the tumor microenvironment," Cancer Res. **56**, 5754–5757 (1996).
34. F. Wahaia, I. Kasalynas, D. Seliuta, G. Molis, A. Urbanowicz, C.D. Silva, F. Carneiro, G. Valusis, and P.L. Granja, "Study of paraffin-embedded colon cancer tissue using terahertz spectroscopy," J. Mol. Struct. **1079**(1), 448–453 (2015).
35. A.A. Gavdush, N.V. Chernomyrdin, K.M. Malakhov, S.T. Beshplav, I.N. Dolganova, A.V. Kosyrkova, P.V. Nikitin, G.R. Musina, G.M. Katyba, and I.V. Reshetov, "Terahertz spectroscopy of gelatin-embedded human brain gliomas of different grades: A road toward intraoperative THz diagnosis," J. Biomed. Opt. **24**(02), 1 (2019).
36. S. Uxa, P. Castillo-Binder, R. Kohler, K. Stangner, G.A. Muller, and K. Engeland, " Ki-67 gene expression," Cell death Differ. (2021).
37. J. Yong, M.F. Zheng, Y. Shugao, J.Y. Chen, and Y.J. Chen, "PTEN and Ki-67 expression isassociated with clinicopathologic features of non-small cell lung cancer," J Biomed Res **28**(06), 462–467 (2014).
38. I. Elmaci, M.A. Altinoz, F.H. Bolukbasi, O. Yapicier, and A. Sav, "Paradoxical results obtained with Ki67-labeling and PHH3-mitosis index in glial tumors: a literature analysis," Clin Neuropathol. **36**(11), 272–282 (2017).
39. L.P. Manasa, M.S. Uppin, and C. Sundaram, "Correlation of p53 and Ki-67 expression with grade and subtype of ependymom," Indian J Pathol Microbiol **55**(3), 308 (2012).
40. J. Zhang, N. Mu, L.H. Liu, J. Xie, H. Feng, J.Q. Yao, T.N. Chen, and W.R. Zhu, "Highly sensitive detection of malignant glioma cells using metamaterial-inspired thz biosensor based on electromagnetically induced transparency," Biosensors and Bioelectronics **185**(2021), 113241 (2021).
41. J.Z. Xu and X.C. Zhang, "Terahertz Technology and Application," Peking University Press (in chinese). (2007).
42. D.W. Parsons, S. Jones, X. Zhang, J.C. Lin, R.J. Leary, P. Angenendt, P. Mankoo, H. Carter, I.M. Siu, and G.L. Gallia, "An integrated genomic analysis of human glioblastoma multiforme," Science **321**(5897), 1807–1812 (2008).
43. D.N. Louis, A. Perry, G. Reifenberger, A. von Deimling, D. Figarella-Branger, W.K. Cavenee, H. Ohgaki, O.D. Wiestler, P. Kleihues, and D.W. Ellison, "The 2016 World Health Organization classification of tumors of the central nervous system: a summary," Acta Neuropathol. **131**(6), 803–820 (2016).
44. P. Zou, H. Xu, P. Chen, Q. Yan, L. Zhao, P. Zhao, and A. Gu, "IDH1/IDH2 mutations define the prognosis and molecularprofles of patients with gliomas: A meta-analysis," PLoS One **8**(7), e68782 (2013).
45. S.T. Qi, L. Yu, S. Gui, Y.Q. Ding, H.X. Han, X.L. Zhang, L.X. Wu, and F. Yao, "IDH mutations predict longer survival and response to temozolomide in secondary glioblastoma," Cancer Science **103**, 269–273 (2013).
46. W. Yan, W. Zhang, G. You, Z. Bao, Y. Wang, Y. Liu, C. Kang, Y. You, L. Wang, and T. Jiang, "Correlation of IDH1 mutation with clinic opathologic factors and prognosis in primary glioblastoma: A report of 118 patients from China," PLoS ONE **7**(1), e30339 (2012).
47. F. Xie, J.J. Tang, X. Wang, Y.H. Liu, and Q. Mao, "Correlation between IDH1 mutation and prognosis in supratentorial high-grade astrocytomas," Sichuan Da Xue Xue Bao Yi Xue Bao. **4**(2), 184–187 (2013).
48. P. Metellus, B. Coulibaly, C. Colin, A.M. de Paula, A. Vasiljevic, D. Taieb, A. Barlier, B. Boisselier, K. Mokhtari, and X.W. Wang, "Absence of IDH mutation identifies a novel radiologic and molecular subtype of WHO grade II gliomas with dismal prognosis," Acta Neuropathol. **120**(6), 719–729 (2010).
49. J.E. Eckel-Passow, D.H. Lachance, A.M. Molinaro, K.M. Walsh, P.A. Decker, H. Sicotte, M. Pekmezci, T. Rice, M.L. Kosel, I.V. Smirnov, G. Sarkar, A.A. Caron, T.M. Kollmeyer, C.E. Praska, A.R. Chada, C. Halder, H.M. Hansen, L.S. McCoy, P.M. Bracci, R. Marshall, S. Zheng, G.F. Reis, A.R. Pico, B.P. O'Neill, J.C. Buckner, C. Giannini, J.T. Huse, A. Perry, T. Tihan, M.S. Berger, S.M. Chang, M.D. Prados, J. Wiemels, J.K. Wiencke, M.R. Wrensch, and R.B.

Biomedical Optics EXPRESS

Jenkins, "Glioma Groups Based on 1p/19q, IDH, and TERT Promoter Mutations in Tumors," N Engl J Med **372**(26), 2499–2508 (2015).
50. W.Q. Chen, Y. Peng, X.K. Jiang, J.Y. Zhao, H.W. Zhao, and Y.M. Zhu, "Isomers Identification of 2-hydroxyglutarate acid disodium salt (2HG) by Terahertz Time-domain Spectroscopy," Sci Rep **7**(1), 12166 (2017).
51. P.Y. Chen, Z.W. Huang, Y.Q. Cao, P.J. Huang, D.B. Hou, and G.X. Zhang, "Terahertz spectral analysis of DNA base molecule cytosine and its methylated structure 5-methylcytosine," Photonics Asia (2019).